3D multi-channel bi-functionalized silk electrospun conduits for peripheral nerve regeneration

ARTICLE *in* JOURNAL OF THE MECHANICAL BEHAVIOR OF BIOMEDICAL MATERIALS · OCTOBER 2014

Impact Factor: 3.42 · DOI: 10.1016/j.jmbbm.2014.09.029

Available online at www.sciencedirect.com

ScienceDirect

www.elsevier.com/locate/jmbbm

Research Paper

3D multi-channel bi-functionalized silk electrospun conduits for peripheral nerve regeneration

T.M. Dinis[a,b,*], R. Elia[b], G. Vidal[a], Q. Dermigny[a], C. Denoeud[a], D.L. Kaplan[b], C. Egles[a,c], F. Marin[a]

[a]BioMécanique et BioIngénierie, UMR 7338, Université de Technologie de Compiègne, France
[b]Department of Biomedical Engineering, Tufts University, Medford, MA, USA
[c]Department of Oral and Maxillofacial Pathology, Tufts University, School of Dental Medicine, Boston, MA, USA

ARTICLE INFO

Article history:
Received 24 July 2014
Received in revised form
25 September 2014
Accepted 30 September 2014
Available online 13 October 2014

Keywords:
Silk
Electrospinning
Bioengineering
Biomechanics
Nerve regeneration

ABSTRACT

Despite technological advances over the past 25 years, a complete recovery from peripheral nerve injuries remains unsatisfactory today. The autograft is still considered the "gold standard" in clinical practice; however, postoperative complications and limited availability of nerve tissue have motivated the development of alternative approaches. Among them, the development of biomimetic nerve graft substitutes is one of the most promising strategies. In this study, multichanneled silk electrospun conduits bi-functionalized with Nerve Growth Factor (NGF) and Ciliary Neurotropic Factor (CNTF) were fabricated to enhance peripheral nerve regeneration. These bioactive guides consisting of longitudinally oriented channels and aligned nanofibers were designed in order to mimic the fascicular architecture and fibrous extracellular matrix found in native nerve. The simple use of the electrospinning technique followed by a manual manipulation to manufacture these conduits provides tailoring of channel number and diameter size to create perineurium-like structures. Functionalization of the silk fibroin nanofiber did not affect its secondary structure and chemical property. ELISA assays showed the absence of growth factors passive release from the functionalized fibers avoiding the topical accumulation of proteins. In addition, our biomimetic multichanneled functionalized nerve guides displayed a mechanical behavior comparable to that of rat sciatic nerve with an ultimate peak stress of 4.0±0.6 MPa and a corresponding elongation at failure of 156.8±46.7%. Taken together, our results demonstrate for the first time our ability to design and characterize a bi-functionalized nerve conduit consisting of electrospun nanofibers with multichannel oriented and nanofibers aligned for peripheral regeneration. Our bioactive silk tubes thus represent a new and promising technique towards the creation of a biocompatible nerve guidance conduit.

*Corresponding author at: CNRS UMR 7338, BioMécanique et BioIngénierie, Centre de Recherche, BP 20529, Rue Personne de Roberval, 60205 Compiègne, France.
E-mail address: tony.dinis@utc.fr (T.M. Dinis).

http://dx.doi.org/10.1016/j.jmbbm.2014.09.029
1751-6161/

1. Introduction

The peripheral nervous system (PNS) transmits information from the central nervous system (brain and spinal cord) to every other part of the body due to motor and sensory neurons (Yan et al., 2009). Injury of the PNS such as a trauma can cause distal atrophy of target muscles or loss of sensation (Li et al., 2013). These peripheral injuries affect 2.8% of trauma USA patients annually. Peripheral nerve damage impacts 200,000 patients in the USA and 300,000 in Europe each year (Belkas et al., 2004; Ichihara et al., 2008). Spontaneous nerve regeneration can occur for nerve gaps smaller than a few millimeters (Bryan et al., 2004), while repairing large gaps (>10 mm) remains a major challenge for surgeons (Dellon and Mackinnon, 1988).

To date, the most effective way to repair large nerve gaps remains autologous nerve grafting. Even if this technique is considered the clinical standard to repair peripheral nerve gaps, there are many limitations, most notably limited donor site availability, morbidity and surgical complications due to the need for two or more operative procedures (Johnson et al., 2013; Liao et al., 2012). For short gaps (<5 mm), biological tissues as arteries, veins or muscle can also be used but these allografts have shown inconsistencies in the effective regenerative ability (Biazar et al., 2010). In recent years, advances have been made to develop new biomaterials as nerve guidance conduits composed of synthetic, natural or composite polymers systems (Hsu et al., 2013; Liu et al., 2012; Masaeli et al., 2013). Despite the fact that the FDA has approved some nerve guidance systems consisting of a variety of different biomaterials such as type I collagen, polyglycolic acid (PGA), poly-DL-lactide-co-caprolactone (PLCL) and polyvinyl alcohol (PVA); the clinical reality is that these biomaterials have not been highly effective for nerve repair after injury or trauma (Kehoe et al., 2012).

Many nerve conduit designs were initially based upon the entubulation model of a porous foam rod or hollow tube (Hadlock et al., 2000; Wang et al., 2006). Unfortunately, using a single hollow guide is not optimal to mimic the proper native spatial arrangement of the ECM and cells within the conduit (Ao et al., 2006). These guidance nerve conduits should facilitate directional axonal growth from the regenerating nerve, protect the regenerating nerve from fibrous tissue barriers and to allow diffusion of growth factors and nutrient exchange. Nerve regeneration can be improved by increasing the surface area for cell growth into the nerve conduit. In addition to architectural design, a prosthetic nerve should present the mechanical and physical properties of in vivo nerve tissues, while include specific properties such as tensile strength, suturability, degradation profile and swelling (Nectow et al., 2012). Surface chemistry is also required to generate conduits that have a high degree of similarity to native tissue. Incorporating growth factors in the biomaterial selected for such designs assures cellular adhesion, viability and promotes neurite outgrowth (Liu et al., 2010; Sahoo et al., 2010a).

Many techniques have been developed to design fibrous scaffolds in order to be used as a tissue substitute. Electrospinning is a fiber spinning technique to produce nanofibers and microfibers under a high-voltage electrostatic field (Inoguchi et al., 2006). Scaffolds prepared via electrospinning, using native and/or synthetic polymers with nanoscale structures similar to native ECM, allow the preparation of aligned fibrous matrix with both adjustable porosity and mechanical properties. Recently, silk electrospun fibers have been applied in the investigation of tissue engineering for biomedical applications (Zhang et al., 2008, 2009). Silk fibroin is a natural protein with good biocompatibility and robust mechanical properties (Altman et al., 2003). The degradation rate of silk biomaterials can also be tailored from months to years after implantation in vivo, based on processing procedures employed during materials formation (Meinel et al., 2005).

Silk fibers can be modified after electrospinning via chemical treatments yielding improved cell proliferation, cell adherence, and growth (Cohen-Karni et al., 2012). Bioactive molecules, such as adhesion or growth factors, can also be added into the spinning solution and remain active and available in the electrospun fibers (Sofroniew et al., 2001). Many different types of bioactive molecules have been incorporated into silk scaffolds of electrospun nanofibers, including growth factors, biomimetic peptides and metals (Li et al., 2006; Sahoo et al., 2010a, 2010b). Growth factors are endogenous proteins capable of binding to cell receptors and directing cellular activities to stimulate the proliferation and differentiation of seeded cells (Varkey et al., 2004). Among multiple growth factors found in the body, neurotrophic factors such as Nerve Growth Factor (NGF) are well known for promoting the survival and differentiation of developing neurons (sensory and sympathetic neurons) in the PNS. The presence of NGF has been demonstrated to enhance neuronal outgrowth and has been used as a chemo-attractant to stimulate axon guidance (Campenot, 1977; Tessier-Lavigne and Goodman, 1996). Another neurotrophic factor produced by Schwann cells, Ciliary NeuroTrophic Factor (CNTF), is abundant in peripheral nerves. CNTF is localized mainly in the cytoplasm of myelinating Schwann cells (Friedman et al., 1992) and its synthesis is decreased during Wallerian degeneration (Rende et al., 1992). It has also been shown that CNTF is a neuroprotective agent and improved the remyelination of regenerated nerves (Kang et al., 2012).

The aim of this article was to design and manufacture nerve guidance conduits based on bi-functionalized 3D silk designs and to define the morphology, growth factors release and mechanical properties to determine if these materials could be a suitable option for nerve prosthesis.

2. Materials and methods

2.1. *Design and manufacture of the bi-functionalized 3D nerve silk conduits*

2.1.1. *Silk fibroin solution preparation*

Silk fibroin was extracted from Bombyx *mori* silkworm cocoons (Tajima Shoji Co., Yojohama, Japan). Solutions were prepared according the following procedure (Rockwood et al., 2011). Cocoons were cut into small pieces (~5 g) and immersed into 2 L of a boiling aqueous solution 0.02 M Na_2CO_3 for 30 min. The degummed fibers were rinsed for 20 min, three times with cold deionized (DI) water, and then allowed to dry for 48 h at room

temperature. Dried silk fibroin fibers were solubilized in 9.3 M LiBr solution (1 g of dried fibers: 4 mL of LiBr solution) at 60 °C for 4 h. Silk solutions were dialyzed against DI water using Slide-a-Lyzer dialysis cassettes (membrane MWCO 3500) (Pierce, Inc., Rockford, IL, USA) for 72 h to remove salts. Silk fibroin solution was centrifuged twice to remove insoluble particulates. The final concentration of aqueous silk fibroin solution was 8 wt%, which was calculated by weighing the remaining solid after drying. The solution was then concentrated by dialyzing against 15% (w/v) PEG for 4 h to produce ≈10 wt% silk fibroin. Silk solutions were stored at 4 °C until used, for never less than 3 weeks.

2.1.2. *Preparation of spinning functionalized solution*

Silk fibroin solutions were mixed with 5 wt% polyethylene oxide (PEO, MW=900 kDa) in a 4:1 ratio to produce a 9% silk/PEO solution. To functionalize the spinning solution, NGF and CNTF (R&D Systems, Inc., Minneapolis, MN, USA) were reconstituted in PBS containing 0.1% bovine serum albumin solution. NGF was added to the silk solution at 100 ng/mL with or without CNTF at 10 ng/mL.

2.1.3. *Electrospinning*

Spinning solution was delivered through a 16G stainless-steel capillary, at a flow rate of 10 μL/min^{-1} using a Sage syringe pump (Thermo Scientific, Waltham, MA). The capillary was maintained at a voltage of 12 kV using a high voltage power supply (Gamma High Voltage Research ES-30P, Ormond Beach, FL, USA) and was mounted at the center of a 10 cm-diameter aluminum plate. To fabricate axial fiber alignment, the collector consisted of a 6 cm-diameter rotating mandrel at 3800 rpm (rotation speed: 10 m/s). The mandrel was positioned 15 cm below the droplet from the spinning solution and covered by silver foil. Electrospun silk-fibroin fibers were collected onto the silver foil. The deposition time was 90 min representing a volume of 1 mL. Fiber alignment was controlled by the rotation speed maintained continuously until the electrospinning process was completed.

2.1.4. *Fabrication of the multichanneled silk nerve conduit*

After 90 min (≈1 mL) of electrospinning, the silver foil was removed from the silk fibers and the electrospun silk mats were stored in dry atmosphere until used. Electrospun fibers mats were rolled up 360°, 50 times using Teflon sticks (0.3 mm diameter) in order to generate a final tube of about 1.0 mm inner diameter (close to a rat sciatic nerve). Teflon sticks were removed after water vapor annealing (Hu et al., 2011) using sterile PBS and then dried. All of the tubes were cut to a length of 1 cm and a diameter of 1 mm.

2.2. *NGF and CNTF release and stability*

NGF and CNTF-functionalized silk nerve conduits were spun with 1 mL of spinning solution at 100 ng/mL and 10 ng/mL (NGF and CNTF respectively). Tubes were incubated in 2 mL of sterile PBS containing 0.1% BSA with 0.02% Tween20 at 37 °C. Then 200 μL of the solution was collected after 1, 6, 24, 72, 168 (CNTF) and 240 h (NGF) and stored at −80 °C. The stability of the two growth factors was assessed during 1 week for CNTF and 10 days for NGF preparing a NGF solution at 500 pg/mL and CNTF solution at 1 ng/mL in sterile PBS containing 0.1% BSA with 0.02% Tween20 at 37 °C. NGF and CNTF release and stability assays were performed with the ChemiKine™ Nerve Growth Factor Sandwich ELISA Kit (Millipore, France) and Raybio® Rat CNTF ELISA kit (TEBU-BIO, France), respectively, according to the manufacturer's instructions.

2.3. *Compliance analysis of the morphology and mechanical properties of the new 3D nerve conduit*

2.3.1. *Morphology and structural analysis*

2.3.1.1. *Scanning electron microscopy*. To analyze the morphology of the new bi-functionalized 3D silk nerve conduits, scanning electron microscopy (SEM) was performed. The electrospun silk functionalized tubes were prepared by cutting thin (1–2 mm) transverse slices of nerve guides with a scalpel and longitudinal slices inside the tubes. SEM samples were sputter-coated with gold/palladium and then evaluated using a field-emission Scanning Electron Microscope (SEM, Supra 55, Zeiss, NY) at 5 kV. To determine channel and fiber diameters and alignment, all SEM images were analyzed by ImageJ and Matlab software packages.

2.3.1.2. *Fourier transform infrared spectroscopy (FTIR)*. FTIR analysis was used to observe the secondary structure of electrospun silk fibers and functionalized electrospun fibers. Analysis of the silk nerve conduits was performed with a Jasco FT/IR-6200 spectrometer (Easton, MD), equipped with a multiple reflection, horizontal Miracle attenuated total reflectance (ATR) attachment (ZnSe crystal, from Pike Tech., Madison, WI). Each measurement incorporated 64 scans with nominal resolution of 4 cm^{-1} (wavenumber from 600 to 4000 cm^{-1}) that were Fourier transformed using a Genzel-Happapodization (ref, details). To identify secondary structures in the protein samples from the absorption spectra, peak positions of the amide I region (1595–1705 cm^{-1}) absorption from Fourier self-deconvolution were analyzed. Curve fitting was performed using Jasco Spectra-Manager Analysis Software (Jasco, Easton MD), as previously described (Hu et al., 2011).

2.3.1.3. *Differential scanning calorimetry (DSC)*. To analyze functionalized polymer properties, DSC was performed. 2 mg of silk nerve guide sample was encapsulated in aluminum pans and heated in a TA Instruments (New Castle, DE) Q100 differential scanning calorimeter (DSC) with purged dry nitrogen gas flow (50 mL/min) and equipped with a refrigerated cooling system. The instrument was calibrated with indium for heat flow and temperature. Aluminum and sapphire reference standards were used for calibration of the heat capacity. Standard mode DSC measurements were performed at a heating rate of 10 °C/min.

2.3.2. *Mechanical behaviour*

2.3.2.1. *Sample preparation*. In order to compare mechanical properties of the sciatic nerve versus our silk nerve implants, Sprague–Dawley (SD) male rats from Janvier Labs, France, were used as a model. All procedures were performed in accordance with the European Directive 2010/63/EU. The rats were housed in the animal unit with 12 h light–12 h dark environment. The average weight of the SD rats aged 12 weeks was 356 g. The animals were euthanized with an

overdose of sodium pentobarbital. After euthanasia, right and left sciatic nerves between the patella and sciatic notch of each rat were removed and then stored in lactate ringer's. For wet silk nerve, the samples were immersed in lactate ringer's during 48 h at room temperature. No preparation was performed for dry silk nerve samples before tensile testing.

2.3.2.2. *Mechanical properties*. Four SD rats (8 nerves) were used to perform tensile tests in order to compare the mechanical properties as per young modulus, maximum load, strain and stress versus silk implants dry or wet. Uniaxial tensile tests were performed by Electroforce 3230 device (Bose Corporation, ElectroForce Systems Group, Minnesota, USA). Tensile tests were performed at room temperature for dry silk nerve conduits whereas rat sciatic nerve and wet silk nerve conduits were performed in a vessel containing 5 L of lactate ringer's. Submerged samples were tested at constant 37 °C temperature, chosen to resemble native rat temperature. The initial gage length for each sample was normalized at 3 mm and an elongation rate of 0.06 mm s^{-1} was applied corresponding to a strain of 2%/s as in previous studies (Ma et al., 2011; Topp and Boyd, 2012). Tensile stress–strain curve, ultimate stress, and elastic modulus were determined by the WinTest software (Bose Corporation, ElectroForce Systems Group, Minnesota, USA) dedicated for this device.

2.4. Statistical analysis

Statistical analysis was performed using InStat software (Software Inc., GraphPad, San Diego, CA). Values were expressed as mean ± standard deviation (mean ± SD). Mechanical properties from each group were compared using nonparametric ANOVA (Kruskal–Wallis Test and Tukey post-hoc test). A p-value less than 0.05 was considered to be significant.

3. Results

3.1. Fabrication of the silk nerve conduit guidance

The electrospinning setup and fabrication process for the 3D silk nerve conduits are illustrated in Fig. 1. Silk fibroin solution was diluted to 8% (w/v) for spinning and NGF and CNTF were added to the spinning solution at 100 ng/mL and 10 ng/mL, respectively. To align the nanofibers, an aluminum mandrel rotating at 9.5 m/s was used into the electrospinning setup

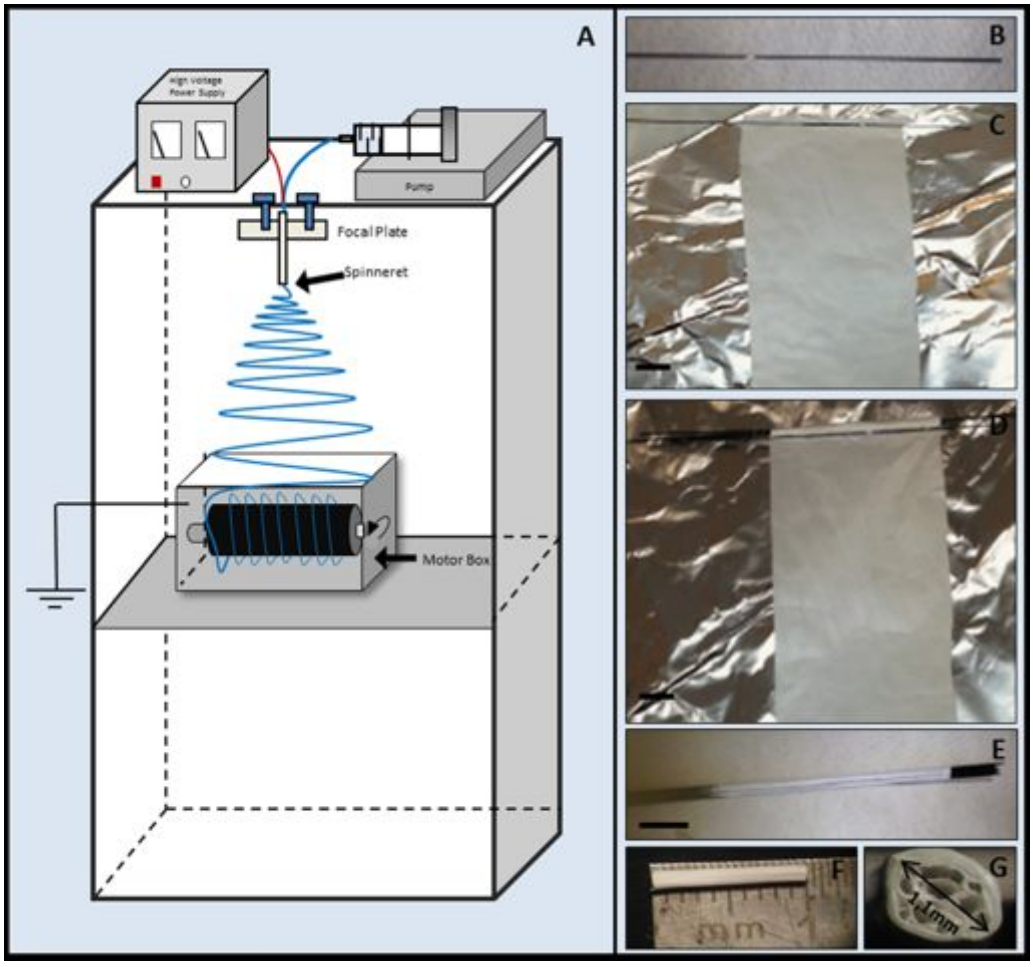

Fig. 1 – Fabrication of 3D silk nerve conduit guidance by electrospinning. Silk aligned nanofibers are collected using an aluminum mandrel rotating at 9.5 m s^{-1} (A) to create a 2D silk aligned nanofibers sheet. Teflon sticks (Ø = 0.3 mm) were used (B) to roll up the silk sheet at 360° (C). This process was repeated for 50 sticks (D). The rest of the silk sheet is rolled up around the structure created (E). All of the tubes fabricated were standardized to a length of 1 cm (F) and a diameter around 1 mm (G). Scale bars: 1 cm.

(Fig. 1A). To form multichannels in the electrospun silk fibers, 0.3 mm diameter Teflon rods were used (Fig. 1B) and 50 sticks were incorporated and rolled up 360° around the silk scaffold one by one (Fig. 1C and D). Once all of the rods were integrated to the mat, the rest of the silk electrospun fibers were used to completely cover the new structure based on a three-dimensional geometric cylinder. This structure had an average inner diameter of 5 mm and a length of 50 mm (Fig. 1E). All tubes formed were treated by water vapor annealing to generate water insoluble silk mats (Hu et al., 2011) overnight and the cylinders were immersed in sterile PBS solution for 5 min in order to remove the Teflon sticks.

Silk guides and bi-functionalized conduits were standardized to 1 mm diameter and 1 cm length (Fig. 1F and G). Of the 160 nerve conduits produced the average length was 1.03±0.1 cm and diameter 1.2±0.2 mm. Their average dry weight was 7.9±2.3 mg.

3.2. *Characterization of morphology*

Representative SEM images of the overall architecture of the silk nerve conduits fabricated are shown in Fig. 2 and show an array of parallel microchannels localized at the center of the tube, enveloped by several layers of silk electrospun fibers. Multichannel guides fabricated are shown in Fig. 2B with approximately 12 channels of different sizes. Eight tubes were used to measure channel diameters localized at the center of the structure and was found to be 183.75±55.9 μm. Lumen areas were also measured with ImageJ software to estimate the material surface area in each section. Lumen area represents 25% of the total tube area, with the remaining 75% composed of the functionalized silk mats. Fig. 2C demonstrates the structure of the electrospun fibers around the microchannels. Nanofiber orientation is well aligned and structured to create an open network of paths for nutrient transport into and out of the channel. Electrospun layers are observed in Fig. 2D which fix the guides into a circular shape consisting of a well-organized network of aligned nanofibers.

Transverse sections of nerve guides were also observed by SEM to characterize fiber diameter and alignment (Fig. 2E) and an average diameter of 792±97 nm was found. The rotating speed applied on the mandrel controlled fiber orientation with 85% of the fibers at an angle of deviation less than 5°. This electrospinning approach provided regular fiber diameter with good alignment. No changes in average diameter or alignment were observed between the silk fiber group and the functionalized (with growth factor) silk fiber group.

3.3. *Growth factor stability and release from electrospun fibers*

The growth factor stability and NGF, CNTF release from the nerve conduits were observed in a PBS-Tween20 solution and determined by ELISA. NGF stability and release were observed over 240 h whereas CNTF over 168 h at 37 °C (Fig. 3).

The 500 pg/mL of NGF was also prepared to observe the degradation rate. The growth factor was stable for the first 72 h and after 168 h 67% of the NGF was detected in the solution, suggesting slow degradation during the first week. At 10 days, less than 15% of the NGF was detected suggesting rapid degradation after 1 week. NGF release from the electrospun silk nerve conduits was detected after the first hour, and then the slope of the curve converged to 0 for a maximal release at 400 pg/mL over 1 week. After one week, slope of the

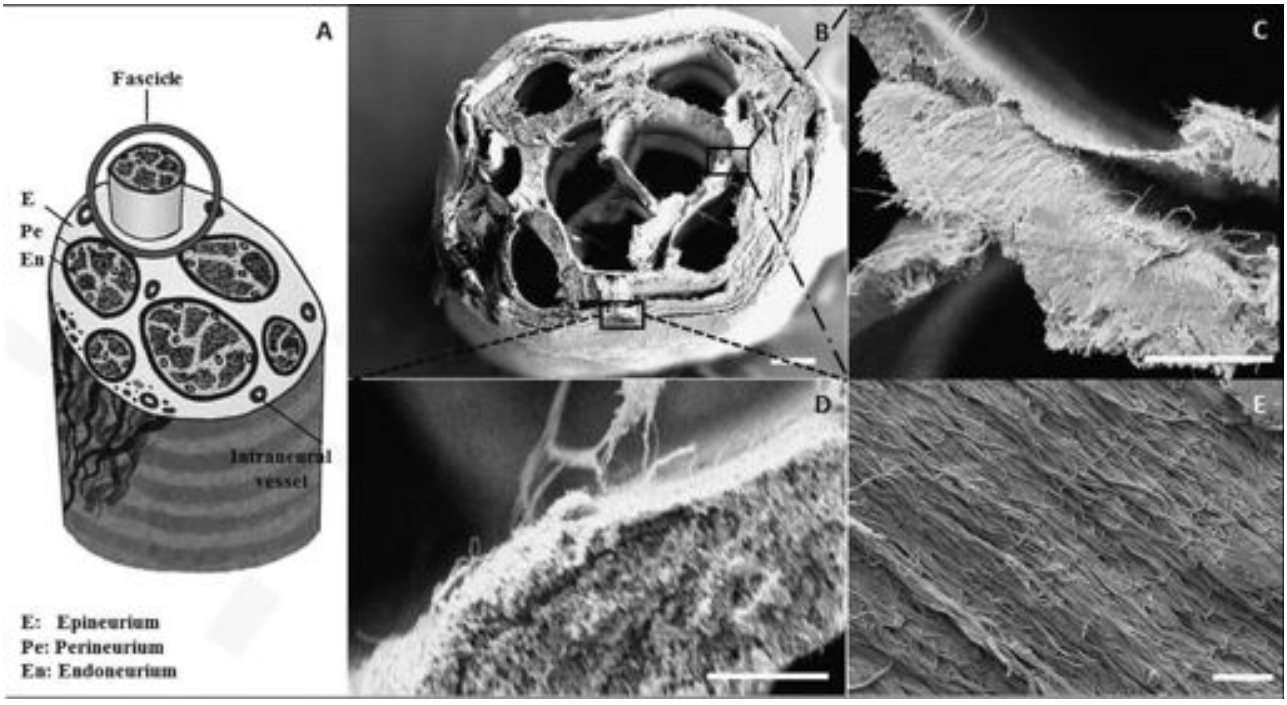

Fig. 2 – Biomimetic comparison of the silk nerve guidance conduit fabricated. Schematic drawing of a peripheral nerve (A). SEM images of microchannels (B: scale bar 200 μm) and nanofibers in the nerve guides (C: scale bar 100 μm and D: scale bar 50 μm). Transverse-section of nerve guide with aligned nanofibers (E: scale bar 10 μm).

curve was negative, showing that the release stopped and degradation of the released growth factors was likely occurring (Fig. 3A). Given that each silk nerve conduit contained 100 ng/mL of NGF, less than 1% of NGF was released from the bi-functionalized silk tubes (Fig. 3B) over these times frames. Therefore, more than 99% of NGF was not released from the conduit over 10 days.

Degradation rate of CNTF was observed using a 1 ng/mL solution. CNTF was stable over the first 3 days, following by rapid degradation from 72 h to 168 h. CNTF release studies showed that 25% of the initial loaded CNTF concentration was detected after 1 week and release from the conduits was not complete at 168 h. After a period of rapid CNTF release during the first 24 h, the release of the growth factor had zero-order release kinetics thereafter. The slope of the curve was stable during these 6 days. These results suggest controlled CNTF release from the silk tubes over a week (Fig. 3C). The total CNTF released from the bi-functionalized nerve conduits was less than 12% after 1 week (Fig. 3C) suggesting that the 88% remaining in the conduit is still active.

3.4. *FTIR/DSC*

FTIR was used to determine if the incorporation of growth factors affected the secondary structure of the silk mats. From Fig. 4A for all silk tubes there were peaks centered at 1625 cm^{-1} corresponding to beta-sheet, characteristic of annealed silk (Hu et al., 2011). As the inset shows there was no significant increase in beta-sheet content between any of the treatments.

The DSC studies revealed that the silk tubes all displayed a similar thermal degradation pattern regardless of growth factor addition. We notice from the three representative DSC curves in Fig. 4B that there was a small endothermic peak around 175 °C, followed by a change in heat flow ~190 °C above the glass transition temperature of uncrystallized silk (178 °C) (Hu et al., 2007). Above this temperature all of the silk samples degraded rapidly, indicating no additional secondary structure crystallization.

3.5. *Mechanical behavior and properties*

Representative stress–strain curves of three groups (rat sciatic nerve, wet silk conduit and dry silk conduit) at same strain rate of 0.02/s are shown in Fig. 5. Mechanical behavior was compared to rat sciatic nerves, which presented three regions (Fig. 5A). The first one is a toe region (typical in most soft tissues) with a low stiffness until 20 % strain, followed by a linear high stiffness region until 50 % strain for 75% of the samples. Then, the stress rapidly decreased after the peak for two thirds of the samples

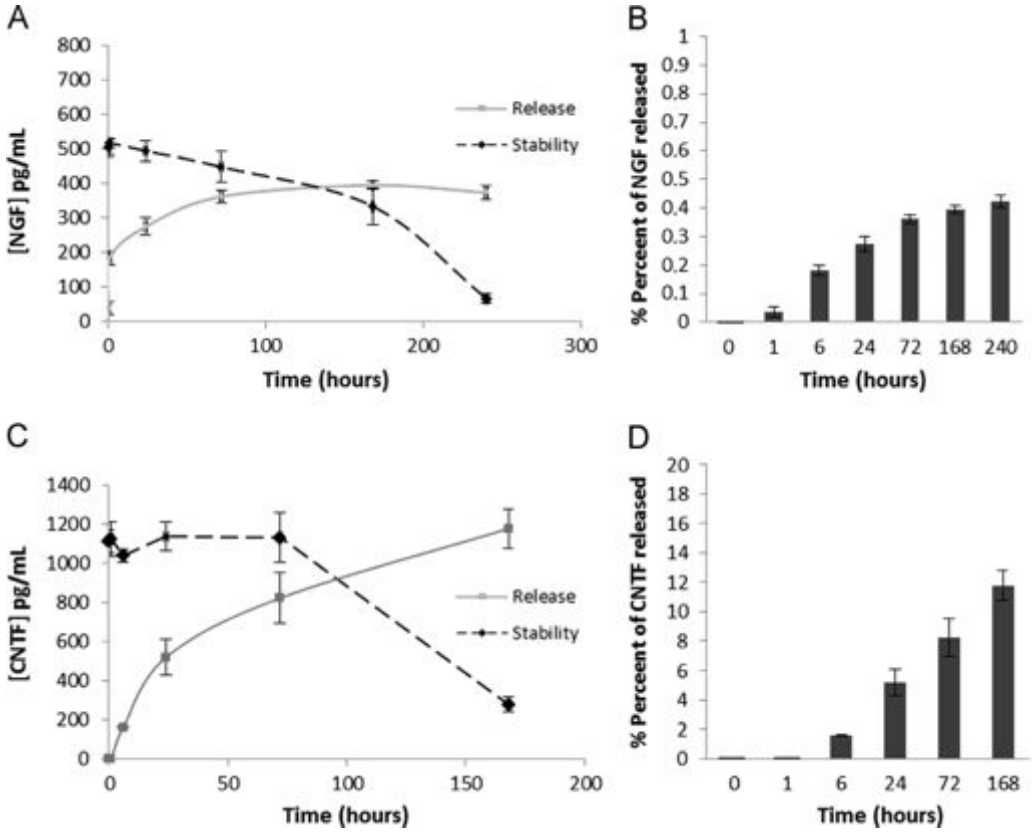

Fig. 3 – Growth factors release from electrospun functionalized silk tubes and stability. (A) Stability: degradation of 500 pg mL^{-1} of NGF was observed in PBS with 0.02% Tween20 during 10 days. After 1 week, more than 65% of NGF could be detected. Release from NGF silk tubes was very low and happened in the day. Then the slope of the curve was decreasing, showing release stopped and growth factors released started to be degraded. (B) Less than 1% of NGF were released from NGF silk tubes. (C) Stability: degradation of 1 ng mL^{-1} of CNTF was observed in PBS with 0.02% Tween20 during 7 days. 25% of CNTF was still detected after 1 week. Release from CNTF silk tubes was not complete during 1 week. (D) Less than 15% of CNTF was released from CNTF silk tubes.

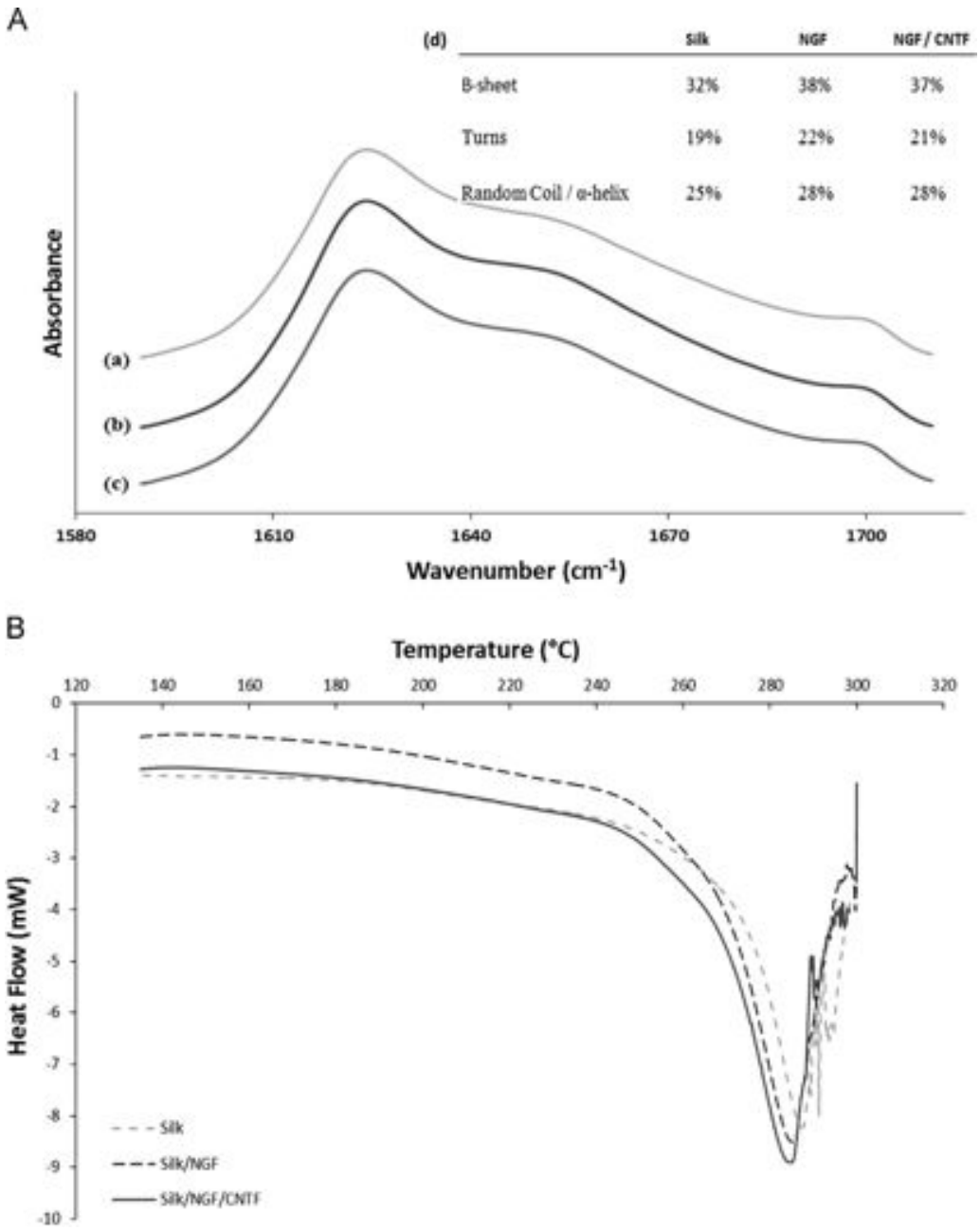

Fig. 4 – FTIR/DSC of silk nerve guidance conduit. (A) FTIR spectra of silk nerve conduit electrospun materials prepared by water annealing. (a) Silk fibroin electrospun; (b) Silk fibroin functionalized with NGF electrospun; (c) Silk fibroin functionalized with NGF and CNTF electrospun. (d) Table of the secondary structure of the nerve conduit. All samples were treated by water-annealing overnight. (B) DSC heating curves of silk nerve conduit, silk functionalized and silk bi-functionalized tubes after water annealing treatment and fully hydratation.

tested. The other third of the samples tested presented a larger failure region and then the stress decreased.

The mechanical behavior of the hydrated conduits also showed the same three regions as the majority of the rat sciatic nerves (Fig. 5B). Curves increased until the peak value, with an initial region up to 25% strain with a higher stiffness compared to regions after this value. For a majority of samples failure regions were after 100% strain. After the peak value, stress decreased intermittently corresponding to successive structural ruptures in the silk construct.

Dry silk nerve conduits exhibited small deformations and were linearly elastic (Fig. 5C). Dry silk allowed a linear high stiffness region until 10%, followed by the permanent plastic deformation until the peak value.

In all the tests, the specimen failure occurred at the midpoint without any observed variations between the samples. Consequently, ultimate stress and failure strain were defined as the values at the peak point of the stress–strain curve. The linear region identified after the toe region was used for the determination of Young's modulus (E).

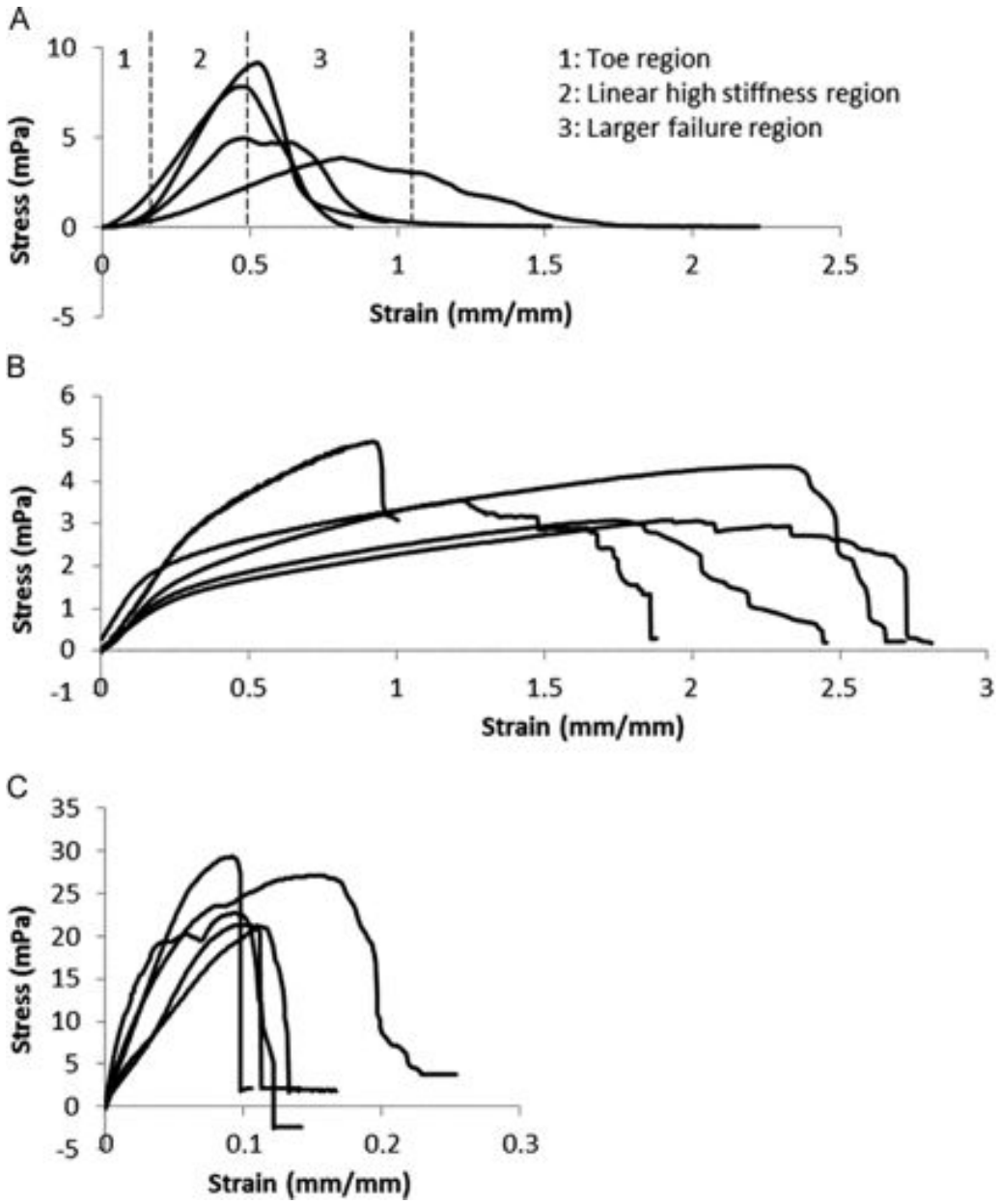

Fig. 5 – Stress=*f*(strain). Comparison of the mechanical behavior of rat sciatic nerve (A), wet (B) and dry (C) silk nerve conduit when subjected to a stretch rate of 0.06 mm/s.

The mechanical properties from tensile tests are summarized in Fig. 6, including force at failure (Max load), failure strain (Max Strain), ultimate stress (Max Stress) and Young's modulus (E).

The force failure of the wet silk conduits was 4.13±0.80 N, not significantly different than the rat sciatic nerves (5.94±2.42 N). The dry silk conduits had force at failure of 23.2±7.1 N which was significantly higher than rat sciatic nerves ($p<0.05$) and wet silk conduits ($p<0.001$) (Fig. 6A). The ultimate strain on wet silk nerve conduits (156.8±46.7%) was not significantly higher than rat sciatic nerves (49.2±2.4%; $p>0.05$) while significantly higher than the dry silk conduits (14±5%; $p<0.001$). The results showed that wet silk conduits could be stretched to more than 100% of original size before failure (Fig. 6B).

Maximum stress obtained for wet silk conduits with 4.0±0.6 MPa was not significantly different than rat sciatic nerves at 6.1±1.5 MPa, while dry silk conduits (25.7±6.2 MPa) were significantly higher than the wet conduit ($p<0.001$) and rat sciatic nerves ($p<0.05$) (Fig. 6C). The elastic modulus of rat sciatic nerves (13.79±5.48 MPa) was not significantly higher than wet silk conduits (8.47±1.33 MPa) while dry silk conduits (331.60±86.4 MPa) were significantly higher than both the wet conduits and rat sciatic nerves ($p<0.05$) (Fig. 6D).

No differences were found between rat sciatic nerves and the hydrated or wet silk conduits for all properties measured, including force applied before failure, stretch, plastic deformation and elasticity.

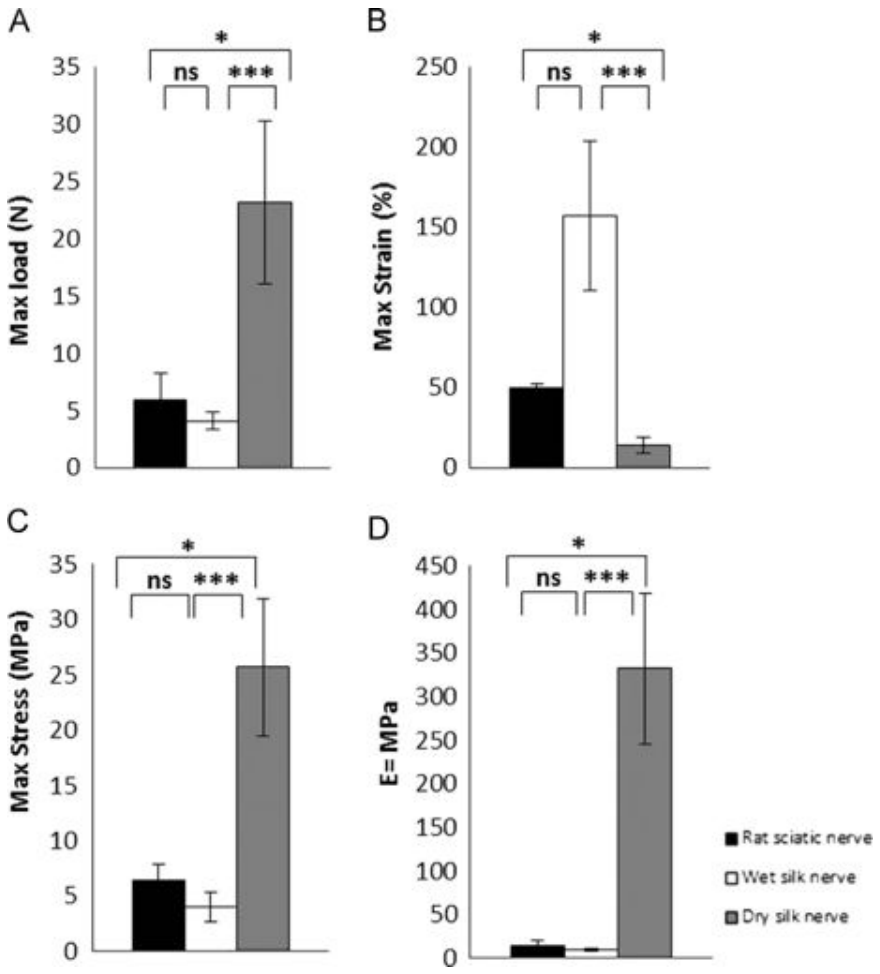

Fig. 6 – Mechanical properties. Mean ± standard deviation values of maximum load (A), maximum strain (B), maximum stress (C) and EE (D) observed on rat sciatic nerve (black), wet silk nerve conduit (white) and dry silk nerve conduit (gray). Standard deviations are shown as error bars. Significant differences (ns: no significance, $^{*}p<0.05$; $^{***}p<0.001$).

4. Discussion

Over the past 30 years no repair strategy has offered the same advantages than the current clinical gold standard for peripheral nerve repair (Geuna et al., 2014; Hadlock et al., 2000). However, the last few years have witnessed significant development of increasingly sophisticated bioengineered nerve graft substitutes composed of synthetic or natural polymer-based nerve guides (Geuna et al., 2014; Lundborg, 2000).

Nerve tissue has a complex architecture where the individual nerve fibers are organized by connective tissue that consists of three distinct components, endoneurium, perineurium, and epineurium. The perineurium delineates different fascicles that look like channels and protects the endoneurium and axons (Fig. 2A). Single channel nerve guides were first fabricated for potential autologous nerve graft replacements (Evans et al., 1991; De Ruiter et al., 2009). However, a single hollow tube may lead to inappropriate targeted reinnervation by the dispersion of regenerating axons across the graft (Brushart et al., 1995; Panseri et al., 2008). Many methods including injection molding (Zeng et al., 2014), freeze drying (Ao et al., 2006; Bozkurt et al., 2007), and electrodeposition (George et al., 2009) have been developed to fabricate multichanneled nerve guides. Moreover, replicating nerve tissues requires an array of parallel and longitudinally oriented microchannels (Stang et al., 2005). In this study, using the electrospinning technique in conjunction with successive Teflon rod molding, a series of multichannel silk conduits with tailored mechanical and chemical properties were fabricated consisting of oriented microchannels composed of aligned functionalized electrospun silk fibers.

Microchannel fabrication of the silk conduits used 10 cm Teflon rods (diameter: 0.3 mm) followed by rolling the functionalized electrospun silk fibers around these rods allows longitudinal aligned microchannels within the guide. Rods were uniform in size but because of the removal under PBS, channel sizes (diameters ranging from 50 to 300 μm) were not uniform as expected. Nevertheless, a high channel density was attained, which may be particularly useful in comparison to other techniques such as mold casting methods (Tran et al., 2014; Yao et al., 2010). Reducing or increasing rod diameter can influence the size of each channel for better control of structure. SEM images in Fig. 2 showed larger primary channels and secondary micro-channels at the center and periphery of the conduits. The channels were maintained by several aligned

functionalized electrospun silk layers to exhibit sufficient interaction to prevent delamination.

Electrospun silk nanofiber scaffolds supported the growth, development and migration of cultured neural cells, with an increase in cell-spreading on small diameters, 400 nm and 800 nm, but not on larger diameters, 1200 nm (Qu et al., 2013). The present silk conduits consisted of aligned nanofibers with an average diameter of 792 nm, suitable for neuron adherence and growth. Electrospun aligned fibers provided topographical cues to direct and enhance neurite outgrowth when compared to random fibers (Corey et al., 2007). In the literature, the unidirectional contours of aligned fibers provided physical guidance to the cells (Lee et al., in press), facilitating axon path finding and accelerating nerve tissue regeneration (Dinis et al., 2013; Liu et al., 2010).

In contrast to existing electrospun nerve guides (Jeffries and Wang, 2012; Mauck et al., 2009; Yucel et al., 2010), our biomimetic design presents a complex three dimensional construct with open channels to guide neurons and Schwann cells between both the aligned microchannels and functionalized fibrous substrate.

Electrospun silk fibers were previously identified as candidate compositions for nerve regeneration based on in vitro studies (Dinis et al., 2013; Wittmer et al., 2011;). Silk biocompatibility and biodegradability are well documented (Duval et al., 2014; Kim et al., 2012; Yang et al., 2007; Zhao et al., 2013). Bioactive molecules can be incorporated into electrospun silk fibers by many methods such as physical adsorption, covalent attachment, co-axial spinneret electrospinning via addition of bioactive molecules into the spinning solution before spinning. NGF and CNTF were added to the spinning solution in order to control the final concentration. The complementary effects of these two growth factors could allow more complete functional nerve regeneration by acting on different subcategories of re-growing fibers. Indeed, NGF is well known to stimulate sensitive fibers whereas CNTF stimulate motors fibers. These dual actions increase the chance of success of obtaining a full functional recovery. Growth factors, in this case, interact with the scaffold mainly through electrostatic interactions (Uebersax et al., 2007). As reported in the literature, we expect a 20% burst release of the factors from electrospun fibers (Sahoo et al., 2010b; Schneider et al., 2009). Interestingly, only 12% of CNTF and 1% of NGF were released from the conduits. At neutral pH, silk fibroin is negatively charged (pI=4.3) and CNTF (pI=5) and NGF (pI=9.3) are positively charged. The molecular weight of NGF (27 kDa) and CNTF (23 kDa) may also impede diffusion. These biophysical factors of charge and size can explain the low release observed in the experiments over one week by ELISA (Uebersax et al., 2007).

The FITR results revealed that there were no differences in secondary structure between functionalized and non-functionalized silk nerve conduits. This can be explained by the fact that all tubes were subject to water vapor annealing in order to make them water insoluble via the induction of crystallization in silk materials (Hu et al, 2011). Thus any changes induced by growth factor addition would be masked by the water vapor annealing process. DSC also confirmed that the protein structure of the three samples was similar. All treatments showed slow degradation above the glass transition temperature of silk followed by rapid degradation above 210 °C. Other studies have demonstrated the same behavior for annealed silk suggesting that the beta-sheet regions account for the observed degradation above the 178 °C glass transition temperature of non-crystalline silk (Hu et al, 2007). No changes on crystallinity demonstrated that functionalized silk exhibited the same polymers properties as the nonfunctionalized silk. Based on previous experience with growth factor incorporation and release from electrospun silk scaffolds (Hu et al., 2011; Li et al., 2006) we did not expect NGF and CNTF incorporation to affect overall beta sheet content, as confirmed by the data.

The mechanical properties of these silk conduits were compared to rat sciatic nerves (Bora et al., 1980; Kwan et al., 1992; Restaino et al., 2014). The native nerve tensile tests showed similar stress–strain behavior and mechanical properties to the rat nerves in previous studies (Ma et al., 2011; Topp and Boyd, 2006), where the epineurium and perineurium were suggested as responsible for the tensile strength. The mechanical properties of the silk conduits were comparable to the rat sciatic nerves as no significant differences were found between the hydrated silk conduits and rat nerves for all biomechanical parameters except for strain. Although, no differences were found for this parameter between the two groups our silk conduits, the values were higher (more stretchable) than native nerves. This characteristic gives these nerve graft substitutes an advantage in terms of handling and suturing during implant surgery. Hydrated and dry silk conduits have shown different mechanical properties due to beta sheet structure (Hu et al., 2011; Jin et al., 2005). Moreover, wet specimen could be a great alternative to ship and store the material before its final use. In our experiments, it is clear they keep mechanical properties that would allow this kind of manipulation.

To summarize, our results demonstrate our ability to create a new bi-functionalized 3D nerve conduits composed of NGF and CNTF electrospun silk nanofibers. They are architecturally biomimetic and able to support and promote PNS nerve regeneration (Dinis et al., 2013). The multichanneled tube is covered both inside and outside by aligned electrospun nanofibers made of a biocompatible and biodegradable silk biomaterial. Moreover, these tubes present compliant mechanical properties to match native nerves. One perspective for the amelioration of this technique is now to avoid any manipulation by hand such as the rolling step involving silk material around Teflon sticks. We are now testing other automated methods offering a better calibration of our design as well as to respect the Current Good Manufacturing Practices requirement for future preclinical trials and marketing authorizations.

5. Conclusions

A method to design nerve conduits for guidance cues consisting of aligned functionalized silk electrospun fibers is described, and the systems can also contain a high density of aligned and longitudinally oriented microchannels mimicking fascicles for peripheral nerve regeneration. The design provides tailored architecture and strength. The conduits were successfully functionalized to provide sustained release of nerve-related growth factors without affecting the silk polymer properties. The nerve graft mechanical

behaviors were comparable to those of rat sciatic nerves. Further studies will focus on the evaluation of these new materials in an in vivo model of sciatic nerve regeneration by motor functionality tests based on the analysis of gait patterns and histological observations.

Acknowledgments

This work was supported by a grant of the region Picardie through the Silknerve Project and the Tissue Engineering Resource Center (TERC, P41 EB002520) from Tufts University. We also thank Sophie Lejay for her collaboration to perform tensile tests. Tony M. Dinis received a fellowship from the French Ministry of Science and Technology.

REFERENCES

Altman, G.H., Diaz, F., Jakuba, C., Calabro, T., Horan, R.L., Chen, J., Lu, H., Richmond, J., Kaplan, D.L., 2003. Silk-based biomaterials. Biomaterials 24, 401–416.

Ao, Q., Wang, A., Cao, W., Zhang, L., Kong, L., He, Q., Gong, Y., Zhang, X., 2006. Manufacture of multimicrotubule chitosan nerve conduits with novel molds and characterization in vitro. J. Biomed. Mater. Res. A 77, 11–18, http://dx.doi.org/10.1002/jbm.a.30593.

Belkas, J.S., Shoichet, M.S., Midha, R., 2004. Peripheral nerve regeneration through guidance tubes. Neurol. Res. 26, 151–160, http://dx.doi.org/10.1179/016164104225013798.

Biazar, E., Khorasani, M.T., Zaeifi, D., 2010. Nanotechnology for peripheral nerve regeneration. Int. J. Nano Dimens. 1, 1–23.

Bora Jr., F.W., Richardson, S., Black, J., 1980. The biomechanical responses to tension in a peripheral nerve. J. Hand Surg. 5, 21–25, http://dx.doi.org/10.1016/S0363-5023(80)80037-2.

Bozkurt, A., Brook, G.A., Moellers, S., Lassner, F., Sellhaus, B., Weis, J., Woeltje, M., Tank, J., Beckmann, C., Fuchs, P., Damink, L.O., Schügner, F., Heschel, I., Pallua, N., 2007. In vitro assessment of axonal growth using dorsal root ganglia explants in a novel three-dimensional collagen matrix. Tissue Eng. 13, 2971–2979, http://dx.doi.org/10.1089/ten.2007.0116.

Brushart, T.M., Mathur, V., Sood, R., Koschorke, G.M., 1995. Joseph H. Boyes Award. Dispersion of regenerating axons across enclosed neural gaps. J. Hand Surg. 20, 557–564.

Bryan, D.J., Tang, J.B., Doherty, S.A., Hile, D.D., Trantolo, D.J., Wise, D.L., Summerhayes, I.C., 2004. Enhanced peripheral nerve regeneration through a poled bioresorbable poly(lactic-co-glycolic acid) guidance channel. J. Neural Eng. 1, 91–98, http://dx.doi.org/10.1088/1741-2560/1/2/004.

Campenot, R.B., 1977. Local control of neurite development by nerve growth factor. Proc. Natl. Acad. Sci. USA 74, 4516–4519.

Cohen-Karni, T., Jeong, K.J., Tsui, J.H., Reznor, G., Mustata, M., Wanunu, M., Graham, A., Marks, C., Bell, D.C., Langer, R., Kohane, D.S., 2012. Nanocomposite gold-silk nanofibers. Nano Lett. 12, 5403–5406, http://dx.doi.org/10.1021/nl302810c.

Corey, J.M., Lin, D.Y., Mycek, K.B., Chen, Q., Samuel, S., Feldman, E.L., Martin, D.C., 2007. Aligned electrospun nanofibers specify the direction of dorsal root ganglia neurite growth. J. Biomed. Mater. Res. A 83, 636–645, http://dx.doi.org/10.1002/jbm.a.31285.

De Ruiter, G.C.W., Malessy, M.J.A., Yaszemski, M.J., Windebank, A.J., Spinner, R.J., 2009. Designing ideal conduits for peripheral nerve repair. Neurosurg. Focus 26, E5, http://dx.doi.org/10.3171/FOC.2009.26.2.E5.

Dellon, A.L., Mackinnon, S.E., 1988. An alternative to the classical nerve graft for the management of the short nerve gap. Plast. Reconstr. Surg. 82, 849–856.

Dinis, T., Vidal, G., Marin, F., Kaplan, D., Eglès, C., 2013. Silk nerve: bioactive implant for peripheral nerve regeneration. Comput. Methods Biomech. Biomed. Eng. 16, 253–254, http://dx.doi.org/10.1080/10255842.2013.815958.

Duval, J.L., Dinis, T., Vidal, G., Vigneron, P., Kaplan, D.L., Egles, C., 2014. Organotypic culture to assess cell adhesion, growth and alignment of different organs on silk fibroin. J. Tissue Eng. Regen. Med.http://dxdoi.org/10.1002/term.1916.

Evans, P.J., Bain, J.R., Mackinnon, S.E., Makino, A.P., Hunter, D.A., 1991. Selective reinnervation: a comparison of recovery following microsuture and conduit nerve repair. Brain Res. 559, 315–321.

Friedman, B., Scherer, S.S., Rudge, J.S., Helgren, M., Morrisey, D., McClain, J., Wang, D.Y., Wiegand, S.J., Furth, M.E., Lindsay, R.M., 1992. Regulation of ciliary neurotrophic factor expression in myelin-related Schwann cells in vivo. Neuron 9, 295–305.

George, P.M., Saigal, R., Lawlor, M.W., Moore, M.J., LaVan, D.A., Marini, R.P., Selig, M., Makhni, M., Burdick, J.A., Langer, R., Kohane, D.S., 2009. Three-dimensional conductive constructs for nerve regeneration. J. Biomed. Mater. Res. A 91, 519–527, http://dx.doi.org/10.1002/jbm.a.32226.

Geuna, S., Tos, P., Titolo, P., Ciclamini, D., Beningo, T., Battiston, B., 2014. Update on nerve repair by biological tubulization. J. Brachial Plex. Peripher. Nerve Inj. 9, 3, http://dx.doi.org/10.1186/1749-7221-9-3.

Hadlock, T., Sundback, C., Hunter, D., Cheney, M., Vacanti, J.P., 2000. A polymer foam conduit seeded with Schwann cells promotes guided peripheral nerve regeneration. Tissue Eng. 6, 119–127, http://dx.doi.org/10.1089/107632700320748.

Hsu, S.H., Chan, S.H., Weng, C.T., Yang, S.H., Jiang, C.F., 2013. Long-term regeneration and functional recovery of a 15 mm critical nerve gap bridged by tremella fuciformis polysaccharide-immobilized polylactide conduits. Evid.-Based Complement. Altern. Med. 2013, 959261, http://dx.doi.org/10.1155/2013/959261.

Hu, X., Kaplan, D., Cebe, P., 2007. Effect of water on the thermal properties of silk fibroin. Thermochim. Acta 461, 137–144, http://dx.doi.org/10.1016/j.tca.2006.12.011(9th Laehnwitzseminar 2006 Special Issue 9th Laehnwithseminar on Calorimetry).

Hu, X., Shmelev, K., Sun, L., Gil, E.S., Park, S.H., Cebe, P., Kaplan, D.L., 2011. Regulation of silk material structure by temperature-controlled water vapor annealing. Biomacromolecules 12, 1686–1696, http://dx.doi.org/10.1021/bm200062a.

Ichihara, S., Inada, Y., Nakamura, T., 2008. Artificial nerve tubes and their application for repair of peripheral nerve injury: an update of current concepts. Injury 39 (Suppl. 4), S29–S39, http://dx.doi.org/10.1016/j.injury.2008.08.029.

Inoguchi, H., Kwon, I.K., Inoue, E., Takamizawa, K., Maehara, Y., Matsuda, T., 2006. Mechanical responses of a compliant electrospun poly(L-lactide-co-epsilon-caprolactone) small-diameter vascular graft. Biomaterials 27, 1470–1478, http://dx.doi.org/10.1016/j.biomaterials.2005.08.029.

Jeffries, E.M., Wang, Y., 2012. Biomimetic micropatterned multi-channel nerve guides by templated electrospinning. Biotechnol. Bioeng. 109, 1571–1582, http://dx.doi.org/10.1002/bit.24412.

Jin, H.J., Park, J., Karageorgiou, V., Kim, U.J., Valluzzi, R., Cebe, P., Kaplan, D.L., 2005. Water-stable silk films with reduced β-sheet content. Adv. Funct. Mater. 15, 1241–1247, http://dx.doi.org/10.1002/adfm.200400405.

Johnson, A.P.P.J., Wood, M.D., Moore, A.M., Mackinnon, S.E., 2013. Tissue engineered constructs for peripheral nerve surgery. Eur. Surg. 45, 122–135, http://dx.doi.org/10.1007/s10353-013-0205-0.

Kang, S.S., Keasey, M.P., Cai, J., Hagg, T., 2012. Loss of neuron-astroglial interaction rapidly induces protective CNTF expression after stroke in mice. J. Neurosci: Off. J. Soc. Neurosci. 32, 9277–9287, http://dx.doi.org/10.1523/JNEUROSCI.1746-12.2012.

Kehoe, S., Zhang, X.F., Boyd, D., 2012. FDA approved guidance conduits and wraps for peripheral nerve injury: a review of materials and efficacy. Injury 43, 553–572, http://dx.doi.org/10.1016/j.injury.2010.12.030.

Kim, J.H., Park, C.H., Lee, O.J., Lee, J.M., Kim, J.W., Park, Y.H., Ki, C.S., 2012. Preparation and in vivo degradation of controlled biodegradability of electrospun silk fibroin nanofiber mats. J. Biomed. Mater. Res. A 100, 3287–3295, http://dx.doi.org/10.1002/jbm.a.34274.

Kwan, M.K., Wall, E.J., Massie, J., Garfin, S.R., 1992. Strain, stress and stretch of peripheral nerve. Rabbit experiments in vitro and in vivo. Acta Orthop. Scand. 63, 267–272.

Lee, J.-H., Lee, Y.J., Cho, H.-J., Shin, H., 2014. Guidance of in vitro migration of human mesenchymal stem cells and in vivo guided bone regeneration using aligned electrospun fibers. Tissue Eng. Part 20 (15–16), 2031–2042.

Li, C., Vepari, C., Jin, H.J., Kim, H.J., Kaplan, D.L., 2006. Electrospun silk-BMP-2 scaffolds for bone tissue engineering. Biomaterials 27, 3115–3124, http://dx.doi.org/10.1016/j.biomaterials.2006.01.022.

Li, R., Hettinger, P.C., Machol, J.A., Liu, X., Stephenson, J.B., Pawela, C.P., Yan, J.G., Matloub, H.S., Hyde, J.S., 2013. Cortical plasticity induced by different degrees of peripheral nerve injuries: a rat functional magnetic resonance imaging study under 9.4 Tesla. J. Brachial Plex. Peripher. Nerve Inj. 8, 4, http://dx.doi.org/10.1186/1749-7221-8-4.

Liao, C.D., Zhang, F., Guo, R.M., Zhong, X.M., Zhu, J., Wen, X.H., Shen, J., 2012. Peripheral nerve repair: monitoring by using gadofluorine M-enhanced MR imaging with chitosan nerve conduits with cultured mesenchymal stem cells in rat model of neurotmesis. Radiology 262, 161–171, http://dx.doi.org/10.1148/radiol.11110911.

Liu, T., Houle, J.D., Xu, J., Chan, B.P., Chew, S.Y., 2012. Nanofibrous collagen nerve conduits for spinal cord repair. Tissue Eng. Part A 18, 1057–1066, http://dx.doi.org/10.1089/ten.TEA.2011.0430.

Liu, X., Chen, J., Gilmore, K.J., Higgins, M.J., Liu, Y., Wallace, G.G., 2010. Guidance of neurite outgrowth on aligned electrospun polypyrrole/poly(styrene-beta-isobutylene-beta-styrene) fiber platforms. J. Biomed. Mater. Res. A 94, 1004–1011, http://dx.doi.org/10.1002/jbm.a.32675.

Lundborg, G., 2000. A 25-year perspective of peripheral nerve surgery: evolving neuroscientific concepts and clinical significance. J. Hand Surg. 25, 391–414, http://dx.doi.org/10.1053/jhsu.2000.4165.

Ma, X.-L., Sun, X.L., Yang, Z., Li, X.L., Ma, J.X., Zhang, Y., Yuan, Z.Z., 2011. Biomechanical properties of peripheral nerve after acellular treatment. Chin. Med. J. 124, 3925–3929.

Masaeli, E., Morshed, M., Nasr-Esfahani, M.H., Sadri, S., Hilderink, J., van Apeldoorn, A., van Blitterswijk, C.A., Moroni, L., 2013. Fabrication, characterization and cellular compatibility of poly (hydroxy alkanoate) composite nanofibrous scaffolds for nerve tissue engineering. PloS One 8, e57157, http://dx.doi.org/10.1371/journal.pone.0057157.

Mauck, R.L., Baker, B.M., Nerurkar, N.L., Burdick, J.A., Li, W.J., Tuan, R.S., Elliott, D.M., 2009. Engineering on the straight and narrow: the mechanics of nanofibrous assemblies for fiber-reinforced tissue regeneration. Tissue Eng. Part B Rev. 15, 171–193, http://dx.doi.org/10.1089/ten.TEB.2008.0652.

Meinel, L., Hofmann, S., Karageorgiou, V., Kirker-Head, C., McCool, J., Gronowicz, G., Zichner, L., Langer, R., Vunjak-Novakovic, G., Kaplan, D.L., 2005. The inflammatory responses to silk films in vitro and in vivo. Biomaterials 26, 147–155, http://dx.doi.org/10.1016/j.biomaterials.2004.02.047.

Nectow, A.R., Marra, K.G., Kaplan, D.L., 2012. Biomaterials for the development of peripheral nerve guidance conduits. Tissue Eng. Part B Rev. 18, 40–50, http://dx.doi.org/10.1089/ten.TEB.2011.0240.

Panseri, S., Cunha, C., Lowery, J., Del Carro, U., Taraballi, F., Amadio, S., Vescovi, A., Gelain, F., 2008. Electrospun micro- and nanofiber tubes for functional nervous regeneration in sciatic nerve transections. BMC Biotechnol. 8, 39, http://dx.doi.org/10.1186/1472-6750-8-39.

Qu, J., Wang, D., Wang, H., Dong, Y., Zhang, F., Zuo, B., Zhang, H., 2013. Electrospun silk fibroin nanofibers in different diameters support neurite outgrowth and promote astrocyte migration. J. Biomed. Mater. Res. A 101, 2667–2678, http://dx.doi.org/10.1002/jbm.a.34551.

Rende, M., Muir, D., Ruoslahti, E., Hagg, T., Varon, S., Manthorpe, M., 1992. Immunolocalization of ciliary neuronotrophic factor in adult rat sciatic nerve. Glia 5, 25–32, http://dx.doi.org/10.1002/glia.440050105.

Restaino, S.M., Abliz, E., Wachrathit, K., Krauthamer, V., Shah, S.B., 2014. Biomechanical and functional variation in rat sciatic nerve following cuff electrode implantation. J. Neuroeng. Rehabil. 11, 73, http://dx.doi.org/10.1186/1743-0003-11-73.

Rockwood, D.N., Preda, R.C., Yücel, T., Wang, X., Lovett, M.L., Kaplan, D.L., 2011. Materials fabrication from Bombyx mori silk fibroin. Nat. Protoc. 6, 1612–1631, http://dx.doi.org/10.1038/nprot.2011.379.

Sahoo, S., Ang, L.T., Goh, J.C.H., Toh, S.L., 2010a. Growth factor delivery through electrospun nanofibers in scaffolds for tissue engineering applications. J. Biomed. Mater. Res. A 93A, 1539–1550, http://dx.doi.org/10.1002/jbm.a.32645.

Sahoo, S., Ang, L.T., Goh, J.C.H., Toh, S.-L., 2010b. Growth factor delivery through electrospun nanofibers in scaffolds for tissue engineering applications. J. Biomed. Mater. Res. A 93, 1539–1550, http://dx.doi.org/10.1002/jbm.a.32645.

Schneider, A., Wang, X.Y., Kaplan, D.L., Garlick, J.A., Egles, C., 2009. Biofunctionalized electrospun silk mats as a topical bioactive dressing for accelerated wound healing. Acta Biomater. 5, 2570–2578, http://dx.doi.org/10.1016/j.actbio.2008.12.013.

Sofroniew, M.V., Howe, C.L., Mobley, W.C., 2001. Nerve growth factor signaling, neuroprotection, and neural repair. Annu. Rev. Neurosci. 24, 1217–1281, http://dx.doi.org/10.1146/annurev.neuro.24.1.1217.

Stang, F., Fansa, H., Wolf, G., Reppin, M., Keilhoff, G., 2005. Structural parameters of collagen nerve grafts influence peripheral nerve regeneration. Biomaterials 26, 3083–3091, http://dx.doi.org/10.1016/j.biomaterials.2004.07.060.

Tessier-Lavigne, M., Goodman, C.S., 1996. The molecular biology of axon guidance. Science 274, 1123–1133.

Topp, K.S., Boyd, B.S., 2006. Structure and biomechanics of peripheral nerves: nerve responses to physical stresses and implications for physical therapist practice. Phys. Ther. 86, 92–109.

Topp, K.S., Boyd, B.S., 2012. Peripheral nerve: from the microscopic functional unit of the axon to the biomechanically loaded macroscopic structure. J. Hand Ther. Off. J. Am. Soc. Hand Ther. 25, 142–151, http://dx.doi.org/10.1016/j.jht.2011.09.002 (quiz 152).

Tran, R.T., Choy, W.M., Cao, H., Qattan, I., Chiao, J.C., Ip, W.Y., Yeung, K.W.K., Yang, J., 2014. Fabrication and characterization of biomimetic multichanneled crosslinked-urethane-doped polyester tissue engineered nerve guides. J. Biomed. Mater. Res. A 102, 2793–2804, http://dx.doi.org/10.1002/jbm.a.34952.

Uebersax, L., Mattotti, M., Papaloïzos, M., Merkle, H.P., Gander, B., Meinel, L., 2007. Silk fibroin matrices for the controlled release of nerve growth factor (NGF). Biomaterials 28, 4449–4460, http://dx.doi.org/10.1016/j.biomaterials.2007.06.034.

Varkey, M., Gittens, S.A., Uludag, H., 2004. Growth factor delivery for bone tissue repair: an update. Expert Opin. Drug Deliv. 1, 19–36, http://dx.doi.org/10.1517/17425247.1.1.19.

Wang, A., Ao, Q., Cao, W., Yu, M., He, Q., Kong, L., Zhang, L., Gong, Y., Zhang, X., 2006. Porous chitosan tubular scaffolds with knitted outer wall and controllable inner structure for nerve tissue engineering. J. Biomed. Mater. Res. A 79, 36–46, http://dx.doi.org/10.1002/jbm.a.30683.

Wittmer, C.R., Claudepierre, T., Reber, M., Wiedemann, P., Garlick, J.A., Kaplan, D., Egles, C., 2011. Multifunctionalized electrospun silk fibers promote axon regeneration in central nervous system. Adv. Funct. Mater. 21, 4202, http://dx.doi.org/10.1002/adfm.201190103.

Yan, H., Zhang, F., Chen, M.B., Lineaweaver, W.C., 2009. Chapter 10: conduit luminal additives for peripheral nerve repair. Int. Rev. Neurobiol. 87, 199–225, http://dx.doi.org/10.1016/S0074-7742(09)87010-4.

Yang, Y., Chen, X., Ding, F., Zhang, P., Liu, J., Gu, X., 2007. Biocompatibility evaluation of silk fibroin with peripheral nerve tissues and cells in vitro. Biomaterials 28, 1643–1652, http://dx.doi.org/10.1016/j.biomaterials.2006.12.004.

Yao, L., Billiar, K.L., Windebank, A.J., Pandit, A., 2010. Multichanneled collagen conduits for peripheral nerve regeneration: design, fabrication, and characterization. Tissue Eng. Part C Methods 16, 1585–1596, http://dx.doi.org/10.1089/ten.TEC.2010.0152.

Yucel, D., Kose, G.T., Hasirci, V., 2010. Tissue engineered, guided nerve tube consisting of aligned neural stem cells and astrocytes. Biomacromolecules 11, 3584–3591, http://dx.doi.org/10.1021/bm1010323.

Zeng, C.G., Xiong, Y., Xie, G., Dong, P., Quan, D., 2014. Fabrication and evaluation of PLLA multichannel conduits with nanofibrous microstructure for the differentiation of NSCs in vitro. Tissue Eng. Part A 20, 1038–1048, http://dx.doi.org/10.1089/ten.TEA.2013.0277.

Zhang, X., Baughman, C.B., Kaplan, D.L., 2008. In vitro evaluation of electrospun silk fibroin scaffolds for vascular cell growth. Biomaterials 29, 2217–2227, http://dx.doi.org/10.1016/j.biomaterials.2008.01.022.

Zhang, X., Reagan, M.R., Kaplan, D.L., 2009. Electrospun silk biomaterial scaffolds for regenerative medicine. Adv. Drug Deliv. Rev. 61, 988–1006, http://dx.doi.org/10.1016/j.addr.2009.07.005.

Zhao, Y., Zhao, W., Yu, S., Guo, Y., Gu, X., Yang, Y., 2013. Biocompatibility evaluation of electrospun silk fibroin nanofibrous mats with primarily cultured rat hippocampal neurons. Biomed. Mater. Eng. 23, 545–554, http://dx.doi.org/10.3233/BME-130775.